

# **BASIC RELATIONS BETWEEN TSUNAMIS CALCULATION AND THEIR PHYSICS–II**

Zygmunt Kowalik  
Institute of Marine Science, University of Alaska  
Fairbanks, AK 99775, USA

## **ABSTRACT**

Basic tsunami physics of propagation and run-up is discussed for the simple geometry of a channel. Modifications of a numerical technique are suggested for the long-distance propagation and for the nonlinear processes in tsunami waves. The principal modification is application of the higher order of approximations for the first derivative in space. Presently, tsunami calculations employ the high resolution 2D and 3D models for generation and runup processes, while propagation is resolved by the regular 2D models. Such approach requires boundary conditions which will seamlessly connect the high resolution calculations to the propagation models. These conditions are described with the help of the method of characteristics.

## 1. Introduction

This is the second part of the paper on relations between tsunami calculations and their physics (Kowalik, 2001, hereinafter, K01). The purpose is to consider modifications of numerical techniques used for the long-distance open ocean propagation and for the upslope propagation. While computing an open-ocean propagation at the resolution of 1 nautical mile (approximately 2km) the numerical dispersion slowly changes tsunami wave parameters by changing amplitude and generating the short dissipative waves. This is especially important for the long-distance deep-ocean propagation of the short-period waves (5min-15min period). To alleviate these numerical effects we suggest using of the higher order of approximations especially for the spatial derivative.

While tsunami wave starts to climb upslope towards the shore the nonlinear advective terms in the equations of motion and the nonlinear terms in the continuity equations start to play important role. Tsunami wave steepens up and starts to break into shorter waves. This dissipative process cannot be fully reproduced through the numerical means because it is connected to the short wave domain, which is not resolved by the applied numerical grid. In this domain the short waves of numerical origin occur along with the physical processes. Neither higher space resolution nor higher time resolution is completely rectifying this problem which starts in the subgrid domain. Application of the simple filter results in deleting the short numerical waves thus allowing to observe how tsunami wave changes while part of its energy is outflowing into the short wave during the tsunami wave breaking. Is this "remnant" tsunami wave is actually observed in nature or only in the computer models? Investigations in this paper and results given by Lynett et al. (2001) show that the physics of the nonlinear processes can be described by numerical solution but the numerical solution needs modifications to take into account the wide spectra of processes.

Applications of the different numerical approaches for the different ocean domains require boundary conditions which will seamlessly connect these domains. A problem to be considered is construction of semi-transparent boundaries. The boundary between oceanic and coastal domains should allow the signal arriving from the ocean to enter the coastal domain without any reflection or dissipation and afterwards when the signal is reflected by shoreline back towards the ocean it must cross the same boundary without any reflections as well. If, for example, such boundary is not completely transparent for tsunami which has entered coastal domain and a portion of the signal is reflected from the boundary back, tsunami will pump energy towards the shore causing permanent increase of the amplitude at the shore. The various conditions at the open boundaries are described with the help of the method of characteristics.

## 2. Numerical approximations for the spatial derivatives.

Consider the numerical solution of the equations of motion and continuity

$$\frac{\partial u}{\partial t} = -g \frac{\partial \zeta}{\partial x} \quad (1)$$

$$\frac{\partial \zeta}{\partial t} = -\frac{\partial}{\partial x}(Hu) \quad (2)$$

Solution of this system is usually searched by the two-time-level or the three-time-level numerical schemes (Kowalik and Murty, 1993a, Imamura, 1996). For construction of the space derivatives in the eqs. (1) and (2), a space staggered grid (Figure 1) is usually used (Arakawa C grid). The two-time-level numerical scheme

$$\frac{(u_j^{m+1} - u_j^m)}{T} = -g \frac{\zeta_j^m - \zeta_{j-1}^m}{h} \quad (3)$$

$$\frac{\zeta_j^{m+1} - \zeta_j^m}{T} = -\frac{(u_{j+1}^{m+1} H_{j+1} - u_j^{m+1} H_j)}{h} \quad (4)$$

is of the second order of approximation in space and only the first order in time. All notations are standard:  $u$  is velocity,  $\zeta$  denotes sea level changes,  $t$  is time,  $x$  denotes horizontal coordinate,  $g$  is the Earth's gravity acceleration ( $g=981 \text{ cm s}^{-2}$ ), and  $H$  is depth.

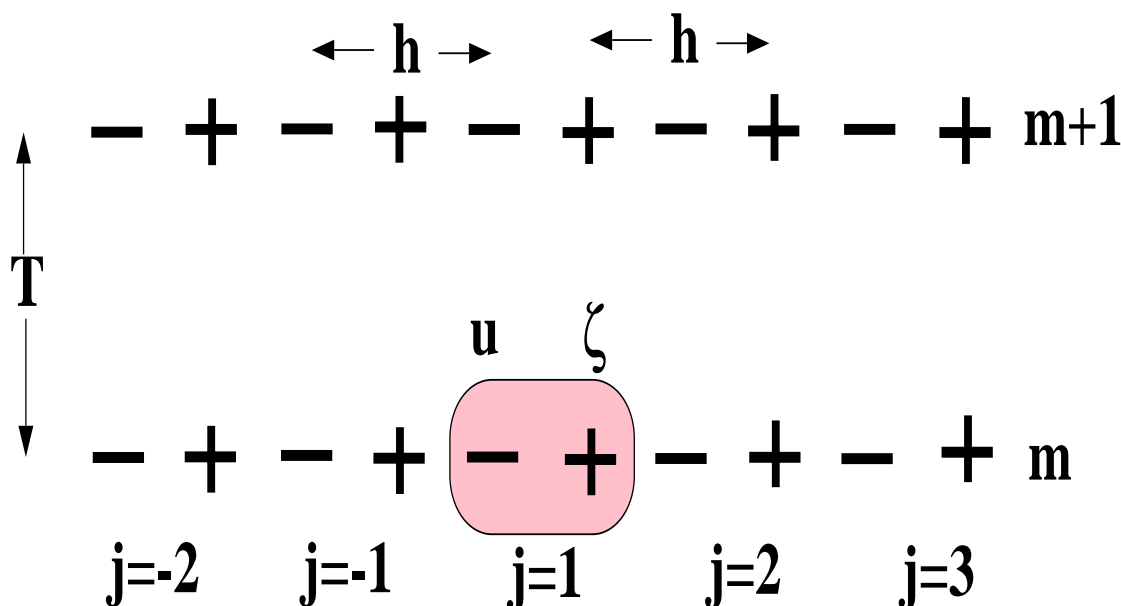


Figure 1

Space-time grid for the tsunami propagation.  $j$  is space index,  $m$  is time index.

The space-staggered grid given in Figure 1 is used to construct space derivatives in the above equations. Variables  $u$  (dashes) and  $\zeta$  (crosses) are located in such a way that the second order of approximation in space is achieved. The depth is taken in the sea level points. The space step along the  $x$  direction is  $h$ . Index  $m$  stands for the time stepping and the time step is  $T$ . Let us consider a simple problem of a sinusoidal wave propagating over the long distance in the channel of the constant depth. At the left end of the channel a sinusoidal wave is given as

$$\zeta = \zeta_0 \sin\left(\frac{2\pi t}{T_p}\right) \quad (5)$$

Here the amplitude is  $\zeta_0=100 \text{ cm}$ , and the period  $T_p$  will be taken from 5 min to 0.5 hour range.

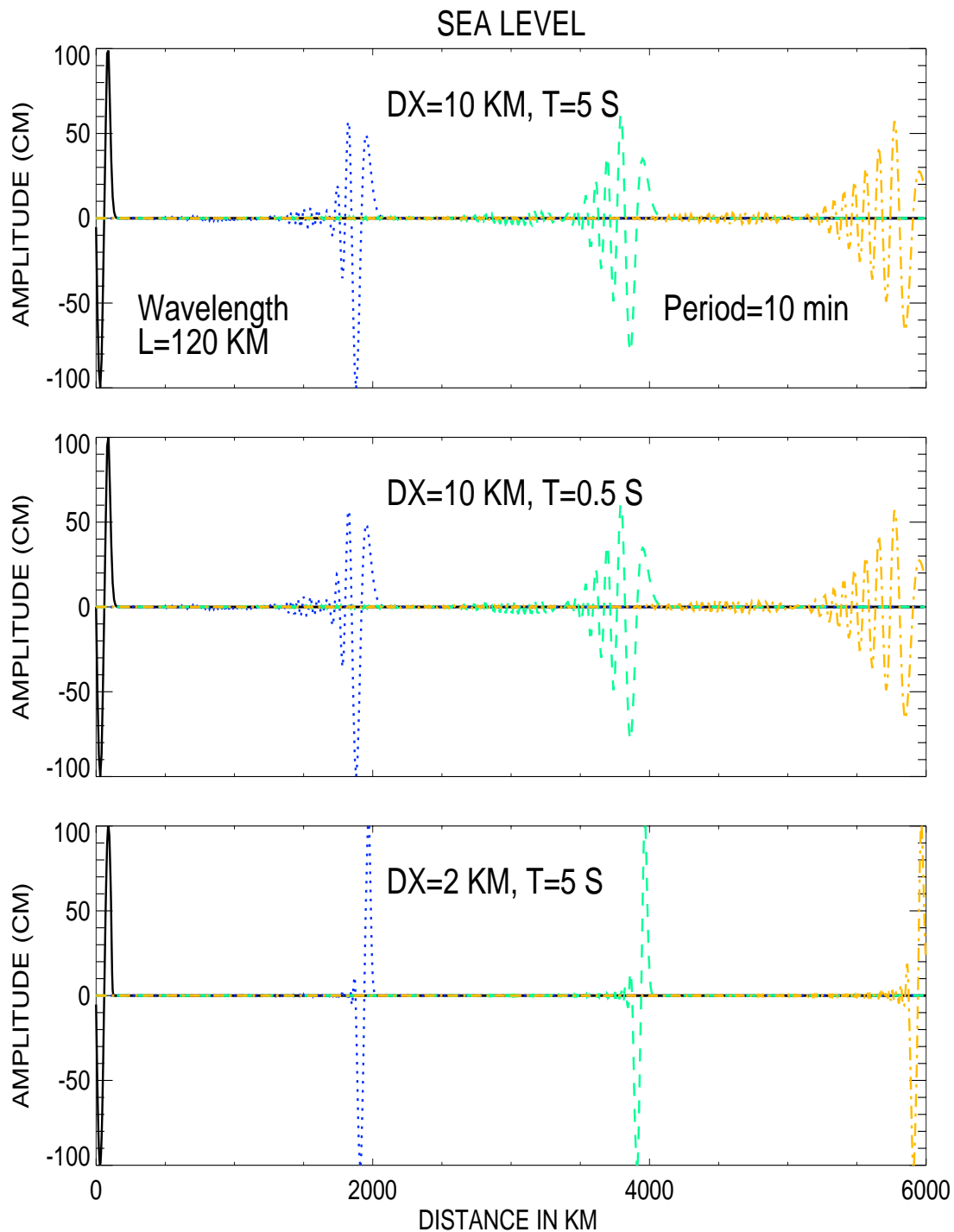


Figure 2

Propagation of the monochromatic wave of 10 min period along the channel of constant 4077 m depth. DX denotes spatial step and T is time step.

Propagation of this monochromatic wave toward the right end of the channel will be studied through eqs. (3) and (4). The right end of channel is open, and a radiating condition will be used so that the wave can propagate beyond the channel without reflection (see eq.(29) Sec. 5, and Reid and Bodine 1968). At the left end of the channel, eq (5) is applied for one period only; after that, the radiating condition is used as well. The channel is 6000 km long and 4077 m deep. The wave period under consideration is 10 min, which results in a 120-km wavelength. The time step of numerical integration will be taken equal to 5 s or 0.5 s. The initial space step is chosen equal to 10 km (close to 5' represented by gridded topography). The 10-km space grid sets 12 steps per wavelength (SPW). Such a resolution will slowly introduce numerical errors into reproduced waves. In Figure 2, results of computation are given for the space step of 10 km (SPW=12) and the time step 5 s (upper panel), for the space step of 10 km and the time step 0.5 s (middle panel), and for the space step of 2 km (SPW= 60) and the time step 5 s (bottom panel). The wave propagation from the left end has been depicted at distances of 2000 km, 4000 km, and 6000 km. The relatively poor space resolution in the upper and middle panels results in the wave damping along the channel.

At approximately 1500 km, the amplitude of the first wave became smaller than the amplitude of the second wave. Traveling wave train has a tail of secondary waves trailing behind the main wave. The shorter time step does not correct dispersive behavior (see the middle panel), only the shorter space step which increases the number of SPW, allows the nondispersive propagation. Dispersive numerical error is cumulative, i.e. for the longer travel distances it will become large enough to generate dispersive waves again. Therefore, the choice of the SPW index will depend on the propagation distance as well.

The time step is aimed at resolving the tsunami wave period and the space step at resolving wavelength. The above discussion shows that the encountered problems are related to the space resolution. This is because we are able to control time resolution but the spatial resolution depends on the resolution of the available bathymetric data. To improve solutions obtained by the numerical methods we shall apply higher order of approximations for the first derivatives in space. We start by constructing the space derivative for the sea level in the equation of motion. The central point ( $u$  point) located in the  $j$  grid point is surrounded by the two sea level grid points at the distance  $h/2$  from the velocity point (see Fig. 1). Consider Taylor series in these points,

$$\zeta_{j+1/2} = \zeta_j = \zeta_j^u + \frac{\partial \zeta_j^u}{\partial x} \frac{h}{2} + \frac{1}{2} \frac{\partial^2 \zeta_j^u}{\partial x^2} \left(\frac{h}{2}\right)^2 + \frac{1}{3!} \frac{\partial^3 \zeta_j^u}{\partial x^3} \left(\frac{h}{2}\right)^3 + \frac{1}{4!} \frac{\partial^4 \zeta_j^u}{\partial x^4} \left(\frac{h}{2}\right)^4 + O(h^5) \quad (6)$$

$$\zeta_{j-1/2} = \zeta_{j-1} = \zeta_j^u - \frac{\partial \zeta_j^u}{\partial x} \frac{h}{2} + \frac{1}{2} \frac{\partial^2 \zeta_j^u}{\partial x^2} \left(\frac{h}{2}\right)^2 - \frac{1}{3!} \frac{\partial^3 \zeta_j^u}{\partial x^3} \left(\frac{h}{2}\right)^3 + \frac{1}{4!} \frac{\partial^4 \zeta_j^u}{\partial x^4} \left(\frac{h}{2}\right)^4 - O(h^5) \quad (7)$$

Along with Taylor series at the distance  $h3/2$ ,

$$\zeta_{j+3/2} = \zeta_{j+1} = \zeta_j^u + \frac{\partial \zeta_j^u}{\partial x} \frac{3h}{2} + \frac{1}{2} \frac{\partial^2 \zeta_j^u}{\partial x^2} \left(\frac{3h}{2}\right)^2 + \frac{1}{3!} \frac{\partial^3 \zeta_j^u}{\partial x^3} \left(\frac{3h}{2}\right)^3 + \frac{1}{4!} \frac{\partial^4 \zeta_j^u}{\partial x^4} \left(\frac{3h}{2}\right)^4 + O(h^5) \quad (8)$$

$$\zeta_{j-3/2} = \zeta_{j-2} = \zeta_j^u - \frac{\partial \zeta_j^u}{\partial x} \frac{3h}{2} + \frac{1}{2} \frac{\partial^2 \zeta_j^u}{\partial x^2} \left(\frac{3h}{2}\right)^2 - \frac{1}{3!} \frac{\partial^3 \zeta_j^u}{\partial x^3} \left(\frac{3h}{2}\right)^3 + \frac{1}{4!} \frac{\partial^4 \zeta_j^u}{\partial x^4} \left(\frac{3h}{2}\right)^4 - O(h^5) \quad (9)$$

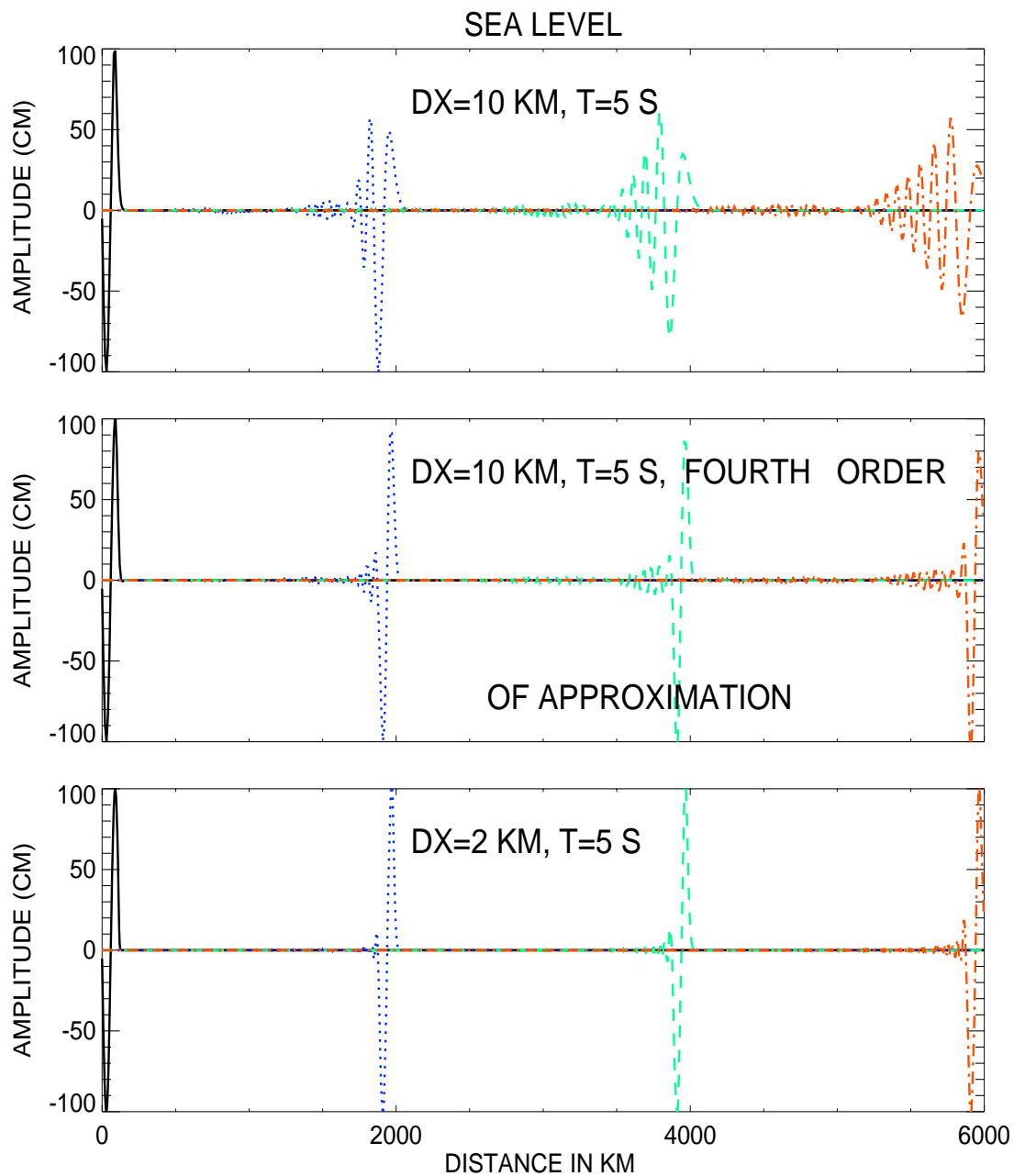


Figure 3

Propagation of the monochromatic wave of 10 min period along the channel of constant 4077 m depth. DX denotes spatial step and T is time step. Middle panel shows application of the higher order derivatives

Here  $\zeta_j^u$  denotes the sea level in the  $u$  point. Space derivative for the sea level in (3) is

obtained by subtracting (7) from (6). Similar formula follows from (8) and (9), but with the longer space step of  $3h$ . The errors (the order of approximation) in both formulas, for the first derivative are proportional to the third derivatives. Thus by combining the two formulas the higher order formula can be constructed. The new formula for the first derivative of the sea level in the  $u$  point reads,

$$\frac{\partial \zeta}{\partial x} = [27(\zeta_j - \zeta_{j-1}) - (\zeta_{j+1} - \zeta_{j-2})]/24h + O(h^4) \quad (10)$$

Space derivative for the velocity in the continuity equation (2) can be constructed in the similar way by noticing that the central point for such derivative is the sea level and the space index should be moved to the right so that  $j$  ought to be substituted by  $j + 1$ . Thus the derivative for the velocity in the  $\zeta$  point reads

$$\begin{aligned} \frac{\partial}{\partial x}(Hu) = \{ & 27[u_{j+1}(h_j + h_{j+1})/2 - u_j(h_j + h_{j-1})/2] - \\ & [u_{j+2}(h_{j+2} + h_{j+1})/2 - u_{j-1}(h_{j-2} + h_{j-1})/2]\} / 24h + O(h^4) \end{aligned} \quad (11)$$

The propagation of the monochromatic wave described with the new derivatives is given in Fig. 3. This is repetition of the Fig. 2 with the middle panel resulting from application the new formulas. It shows essential improvement when compared against the results obtained with the second order derivatives (upper panel).

### 3. Propagation in sloping channel

We shall proceed to construct a simple algorithm for the propagation along the up-sloping channel as we did in the previous paper (K01). This numerical scheme allows us to investigate processes occurring across the shelf. We will be able to pinpoint the influence of friction and nonlinear terms on the process of propagation and dissipation and hopefully understand how numerical schemes change tsunami physics. Consider equation of motion and continuity along  $x$  direction:

$$\frac{\partial u}{\partial t} + u \frac{\partial u}{\partial x} = -g \frac{\partial \zeta}{\partial x} - \frac{ru|u|}{D} \quad (12)$$

$$\frac{\partial \zeta}{\partial t} = \frac{\partial}{\partial x}(Du) \quad (13)$$

Solution of this system will be searched through the two-time-level numerical scheme. The nonlinear (advective) term will be approximated by the upwind/downwind scheme.  $D$  in the above equations denotes the total depth  $D = H + \zeta$ .

The following numerical scheme is used to march in time:

$$\begin{aligned} \frac{(u_j^{m+1} - u_j^m)}{T} + up \frac{(u_j^m - u_{j-1}^m)}{h} + un \frac{(u_{j+1}^m - u_j^m)}{h} \\ = -g \frac{(\zeta_j^m - \zeta_{j-1}^m)}{h} + \frac{ru_j^m |u_j^m|}{0.5(D_j^m + D_{j-1}^m)} \end{aligned} \quad (14)$$

Here:  $up = 0.5(u_j^m + |u_j^m|)$ , and  $un = 0.5(u_j^m - |u_j^m|)$

$$\frac{\zeta_j^{m+1} - \zeta_j^m}{T} = -[(u_{j+1}^{m+1} 0.5(D_j^m + D_{j+1}^m) - u_j^{m+1} 0.5(D_{j-1}^m + D_j^m)]/h \quad (15)$$

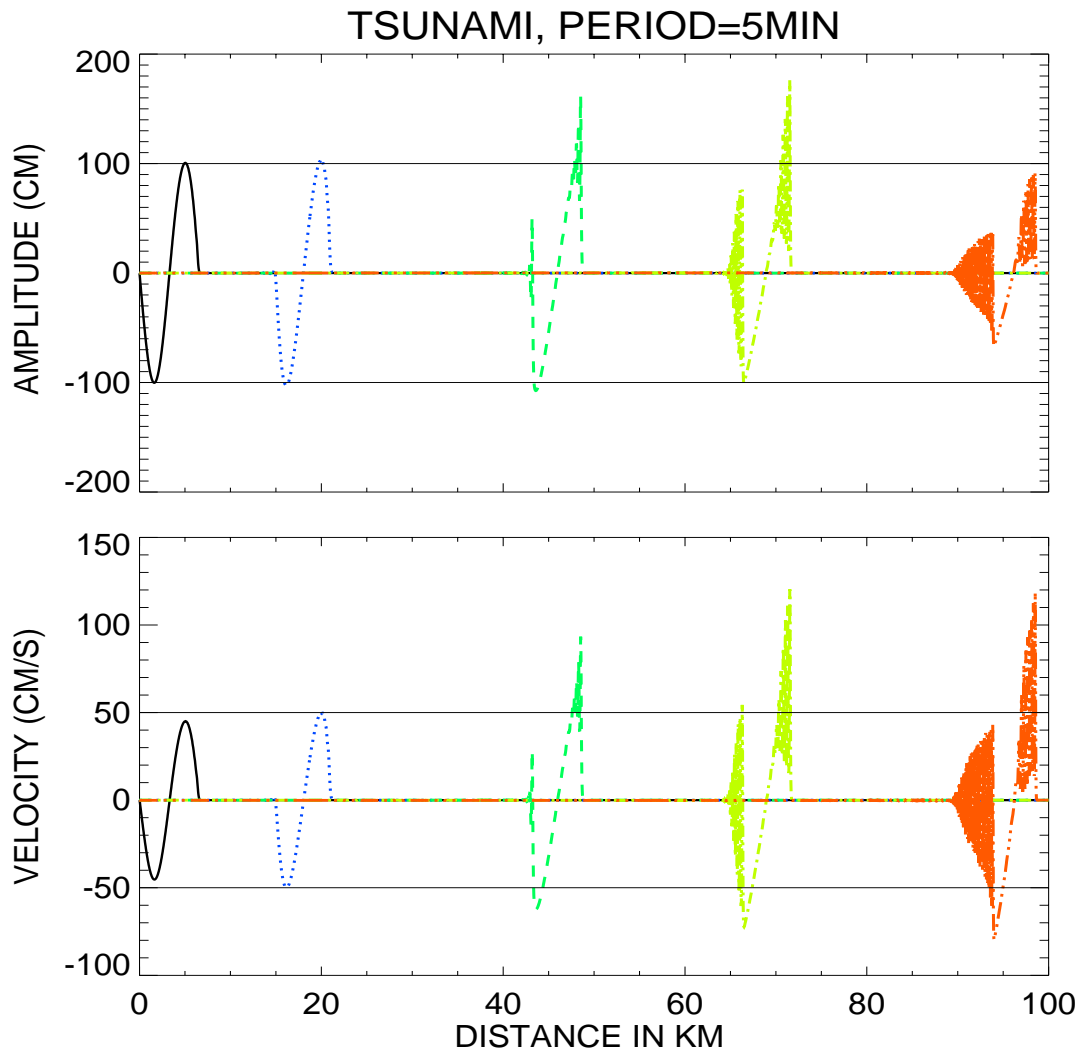


Figure 4

Amplitude (upper panel) and velocity (lower panel) of 5 min period wave. Advective term and bottom friction are included.

In this experiment the upsloping channel of 100 km length is considered. Depth is changing from 50 m at the entrance to 5 m at the end of the channel. We start by computing propagation of a 5 min period tsunami wave from the deep water towards the shallow water. Results we had obtained previously are depicted again in Fig.4. Again, it is important to notice the large disparity in the sea level and velocity. While the sea



level amplitude changes over a small range along the channel, velocity, on the other hand, displays much greater variations and is less prone to the dissipation. The wider range of changes in the velocity field offers better opportunity to compare models and observations. The comparison of the models against the sea level amplitude only, often show that the lack of the bottom friction results in an increase of the amplitude, but the results are not very different from the frictional models (Titov and Synolakis, 1998).

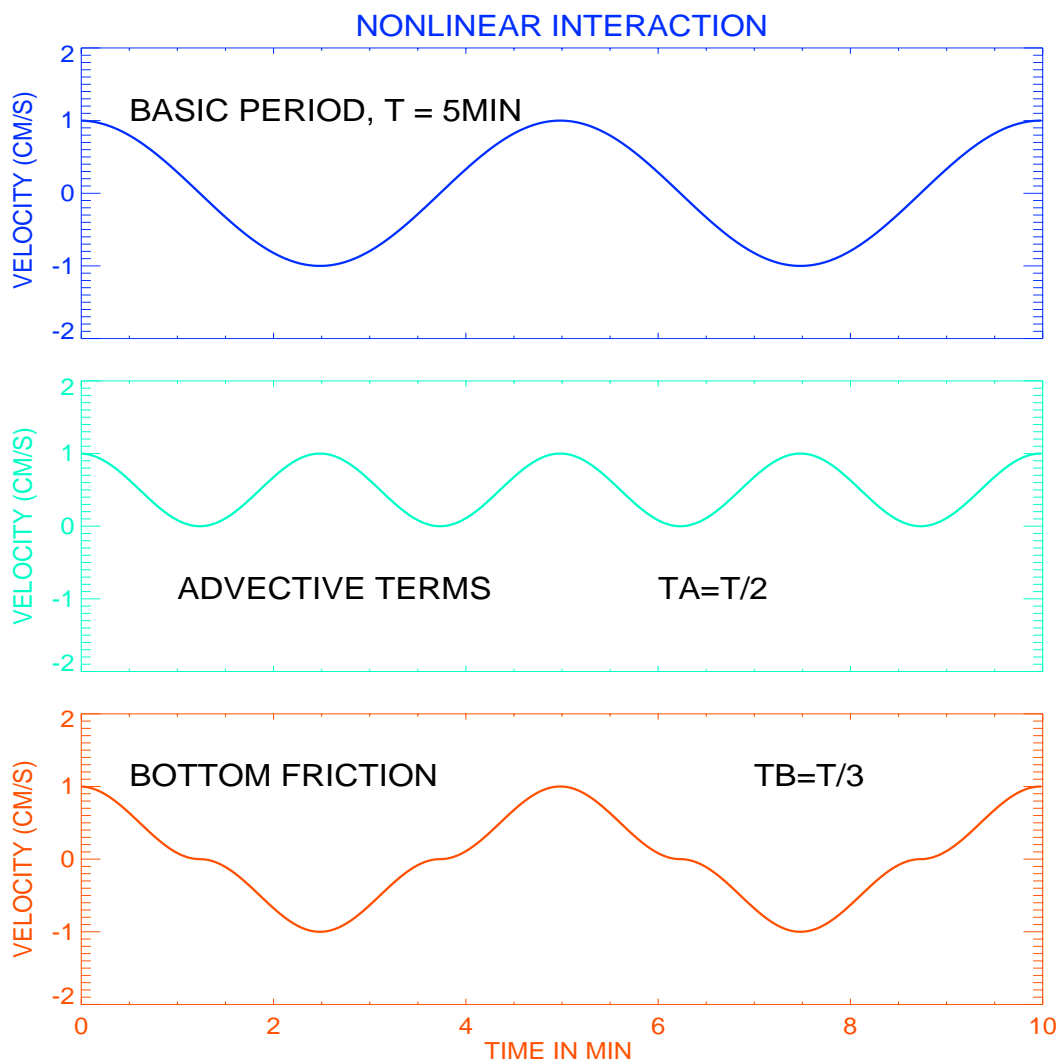


**Figure 5**

**Velocity wave of the unit amplitude (upper panel). The nonlinear wave produced by the advective term (middle panel) and by the bottom friction (lower panel)**

Here we investigate the wave breaking process in the upsloping channel. Is this true physical process of the long wave breaking or this is a numerical artifact? The period is 600 s and the time step 0.1 s, thus the temporal resolution is 6000SPP (step per period).

The wavelength is changing from approximately 7 km at the 50 m depth to 2 km at the 5 m depth. The latter is resolved with 25 m grid resulting in 80SPW, which is still an excellent resolution. Unfortunately, a simple notion of the spatial and temporal resolution needs to be reexamined since in the shallow water a strong nonlinear interaction occurs. This phenomenon should change our approach to analyzing the numerical stability of the basic set of equations, because previously we relied on the linear stability analysis only. Strong nonlinearities are often source of computational instabilities (Lewis and Adams, 1983). It follows from Fig.4 that even if the entire spectra of incident waves is limited to only one period the nonlinear interactions should result in the new periods and in the rectified current. The average velocity calculated over an incident wave period is not equal to zero, resulting therefore in the rectified currents. Let's consider a wave of the unit amplitude in velocity and of the 5 min period (Fig. 5, upper panel) and calculate the influence of the advective terms (middle panel) or the bottom friction terms (lower panel). The new period in the middle panel is 2.5 min, and in the bottom panel is 1.67 min. Generally, the wave of the period  $T$  generates through the advective terms the new oscillations whose periods are  $T_A = T/2i$ , where  $i = 1, 2, 3, \dots$ . The new periods due to the bottom friction are  $T_B = t/(2i + 1)$ , where  $i = 1, 2, 3, \dots$  (Parker, 1991). It is of interest to notice that the amplitude of the secondary oscillations in the lower panel is significantly smaller than the amplitude of oscillations in the middle panel. Conclusion is that the advective mechanism more effectively transfers linear motion into the nonlinear motion. The process of breaking longer waves into shorter waves proceeds continuously, thus the waves shown in Fig. 5 will break into the shorter period waves as well. To test whether the short period waves are the part of physical phenomenon we carry out a simple experiment with an improved spatial resolution by taking step  $h=5\text{m}$ . The result of calculation is given in Fig. 6. In the upper panel for comparison the result with  $h=25\text{ m}$  is also shown.

The improvement in resolution (lower panel) leads to decreasing of the short wave oscillations. Therefore, we may conclude that the short wave oscillations is an computational artifact caused by the poor space resolution. The main source of nonlinear effects is advective term. To the advective term in eq. (14) the upwind method of the first order approximation in space is applied. The upstream approach is used for the stability reason. To deal with stability problems even with the higher order of approximation for the first derivatives (see Kowalik and Bang, 1987, Kowalik and Murty, 1993a) the upstream approach is needed. Construction of the first derivative can be carried out on the three-point or four-point stencil. For the three-point stencil the following construction can be used for the advective term,

$$u \frac{\partial u}{\partial x} \simeq up \frac{(3u_j^m - 4u_{j-1}^m + u_{j-2}^m)}{2h} + un \frac{(-u_{j+2}^m + 4u_{j+1}^m - 3u_j^m)}{2h} + O(h^3) \quad (16)$$

Application of this approach to the advective term together with the higher order derivatives (10) and (11) for the remaining space derivatives leads again to the improved results shown in the lower panel of Fig. 7.

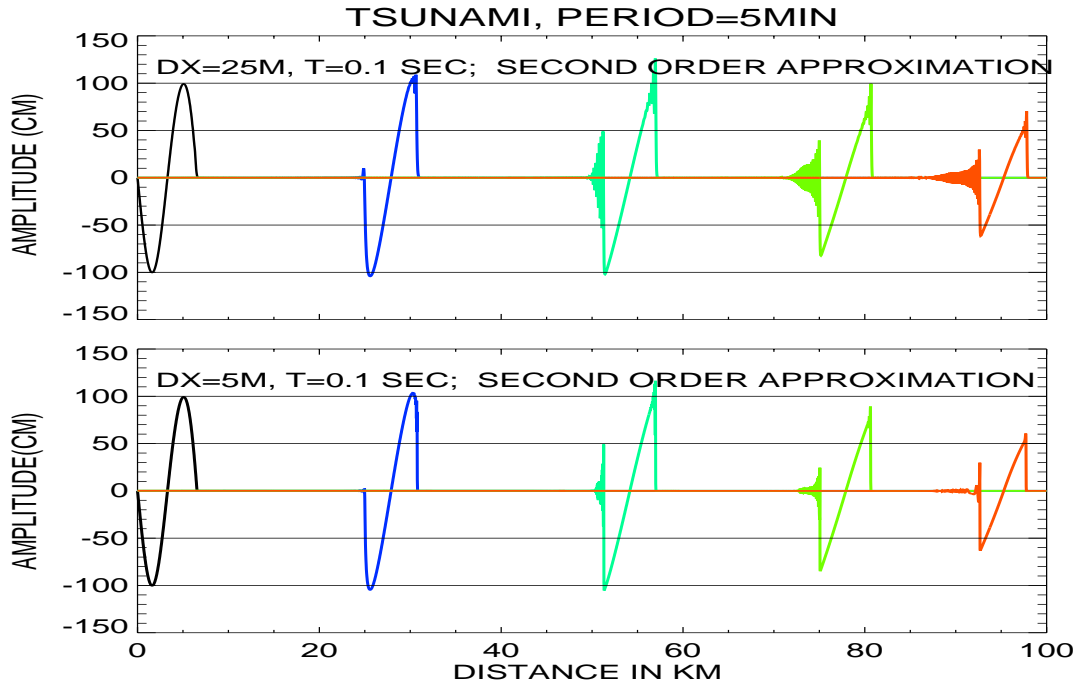


Figure 6

Wave traveling in upsloping channel. Solution obtained by eqs. (14) and (15). Upper panel: space step 25 m, lower panel: space step 5 m.

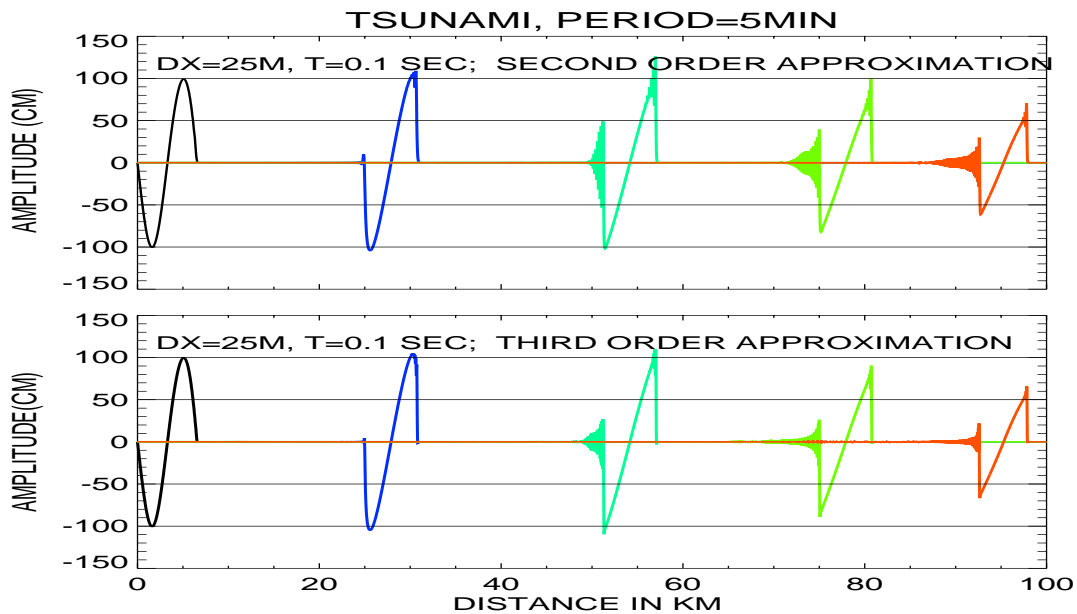


Figure 7

Wave traveling in upsloping channel. Upper panel: solution by eqs. (14) and (15), lower panel: solution by the third order approximation

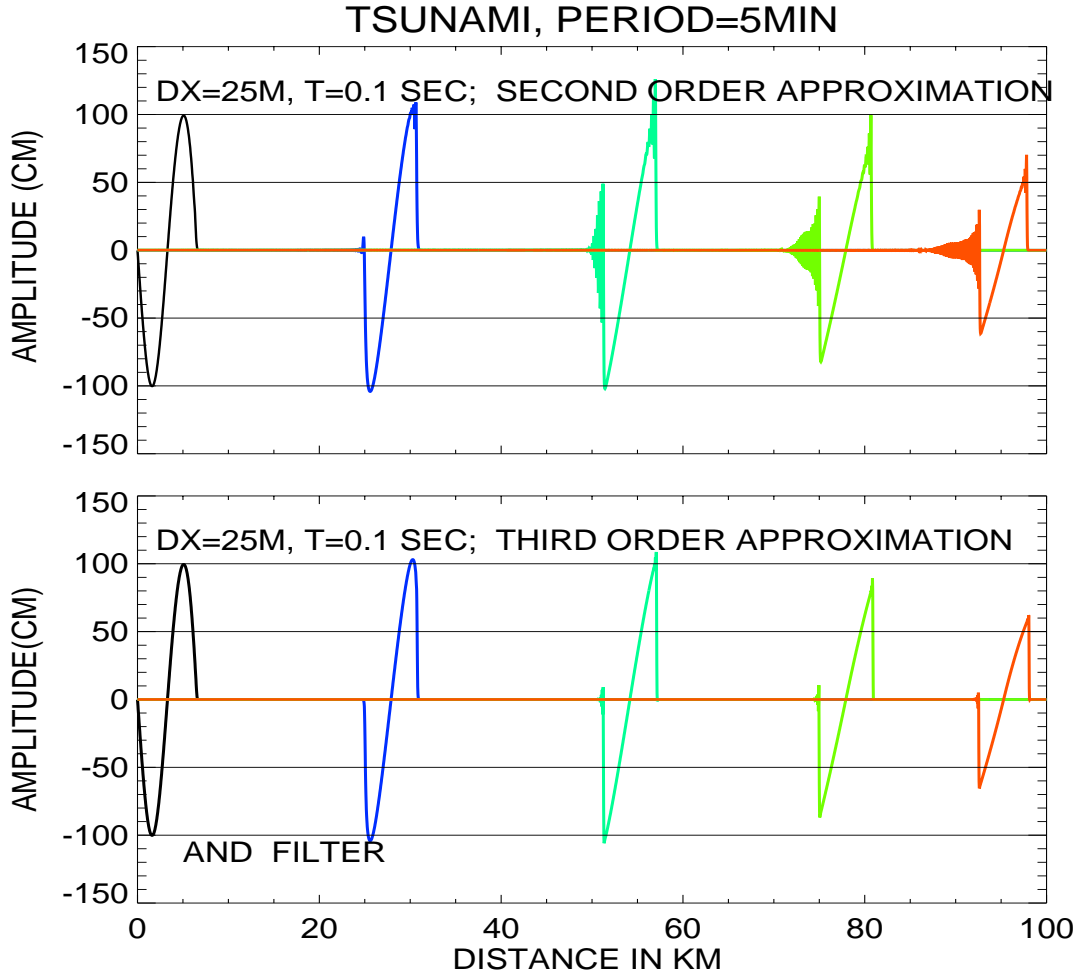


Figure 8

Wave traveling in upsloping channel. Upper panel: solution by eqs. (14) and (15), lower panel: solution by the third order approximation and space filter

Conclusion from the above experiments is that the parasitic short wave oscillations can be deleted through an application of the high spatial and temporal resolutions. A somewhat different and easier solution is application of a simple space filter. It is applied only to the computed velocity. The new velocity  $u_j^{m+1}$  is filtered in the following manner,

$$UN(J) = u_j^{m+1} * (1 - ALP) + 0.25 * (u_{j-1}^{m+1} + 2 * u_j^{m+1} + u_{j+1}^{m+1}) * ALP \quad (17)$$

The filter parameter  $ALP = 0.005$ . The computation carried out with the high order derivatives and the above filter are shown in the lower panel of Fig. 8

#### 4. Run-up in channel

We use here the algorithm previously given in K01, see also Kowalik and Murty, (1993b). The equation of motion is solved by (14), while the continuity equation is approximated by the upwind/downwind approach as well. This approach introduced by Mader (1986) makes equation of continuity quite stable at the boundary between wet and dry domains. The following numerical scheme is used to march in time for the equation of continuity:

$$\frac{\zeta_j^{m+1} - \zeta_j^m}{T} = -(upj1 \times D_j^m + unj1 \times D_{j+1}^m - upj \times D_{j-1}^m - unj \times D_j^m) \quad (18)$$

In the above equation:

$$upj1 = 0.5(u_{j+1}^{m+1} + |u_{j+1}^{m+1}|) \quad \text{and} \quad unj1 = 0.5(u_{j+1}^{m+1} - |u_{j+1}^{m+1}|)$$

$$upj = 0.5(u_j^{m+1} + |u_j^{m+1}|) \quad \text{and} \quad unj = 0.5(u_j^{m+1} - |u_j^{m+1}|)$$

To simulate the run-up and run-down, the variable domain of integration is established after every time step by checking whether the total depth is positive. This was done through a simple algorithm proposed by Flather and Heaps (1975) for the storm surge computations. To answer whether  $u_j$  is a dry or wet point, the sea level is tested at this point;

$$\begin{cases} u_j \text{ is wet point,} & \text{if } 0.5(D_{j-1} + D_j) \geq 0; \\ u_j \text{ is dry point,} & \text{if } 0.5(D_{j-1} + D_j) < 0 \end{cases} \quad (19)$$

Figure 9, middle and lower panels, describes an experiment in which 15 min and 30 min period waves of 1 m amplitude are continuously generated at the open end of the channel.

After this signal is reflected from the sloping boundary, a standing wave is settled in the constant bottom domain. One can glean from this figure that the runup for the 15 min period is much bigger than the runup for the 30 min. Such growth usually show conditions close to the resonance. The sea level distribution in the channel depends strongly on the open boundary condition used for the computation. Setting only velocity or sea level at the open boundary may generate an additional error. The boundary condition must be semi-transparent. With the help of such boundary condition we should be able to set required sea level (or velocity) at the boundary and when the incident wave reflects from a shore and arrives to the open boundary it should cross the boundary without any reflections. These boundary conditions are discussed in the next sections.

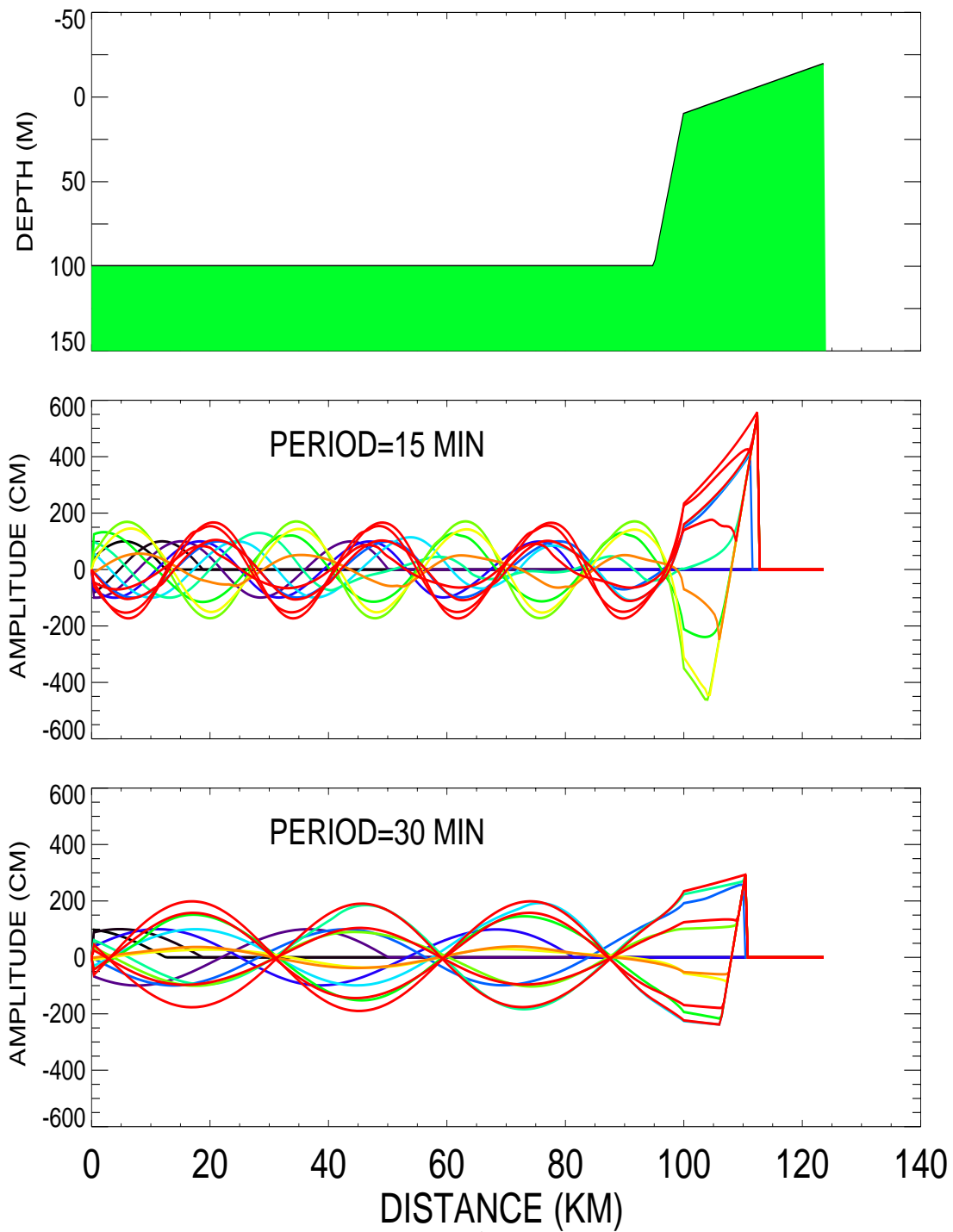


Figure 9

Upper panel: depth distribution. Propagation of 1 m amplitude wave: Middle panel: 15 min period, lower panel: 30 min period.

## 5. Boundary conditions for the tsunami problems

Presently, to calculate tsunami generation and runup the high resolution 2D or 3D models are used, while the open ocean physics is well resolved by 2D models. To construct a boundary condition for connecting the propagation and generation domains let's consider first a simple flow in a channel described by eqs. (1) and (2).

Introducing solution in the form  $(u, \zeta) = (u_0, \zeta_0)\Phi(x - ct)$  into these equations gives rise to a simple set

$$-cu_0 + g\zeta_0 = 0 \quad (20)$$

$$Hu_0 - c\zeta_0 = 0, \quad (21)$$

whose solution defines the well known dispersion relation  $c = \pm\sqrt{gH}$ .

Solutions to eqs.(1) and (2) can be written now as superposition of two waves traveling into positive and negative directions along the x axis,

$$\zeta = \zeta_0^+ \Phi(x - ct) + \zeta_0^- \Phi(x + ct) \quad (22)$$

$$u = u_0^+ \Phi(x - ct) + u_0^- \Phi(x + ct) \quad (23)$$

Through eq.(20) and (21) the velocity amplitudes are related in the following way to the sea level amplitudes

$$u_0^+ = \sqrt{\frac{g}{H}}\zeta_0^+ \quad \text{and} \quad u_0^- = -\sqrt{\frac{g}{H}}\zeta_0^- \quad (24)$$

With this substitution eq.(23) reads,

$$u = \sqrt{\frac{g}{H}}\zeta_0^+ \Phi(x - ct) - \sqrt{\frac{g}{H}}\zeta_0^- \Phi(x + ct) \quad (25)$$

Combining eqs.(22) and (23) the two dependent variables  $u$  and  $\zeta$  are expressed by two disturbances  $\zeta_0^+ \Phi(x - ct)$  and  $\zeta_0^- \Phi(x + ct)$  which we denote as  $\Phi_+$  and  $\Phi_-$ . Through eqs.(22) and (25) these functions are expressed as

$$\Phi_+ = \frac{\zeta + u\sqrt{H/g}}{2} \quad (26a)$$

$$\Phi_- = \frac{\zeta - u\sqrt{H/g}}{2} \quad (26b)$$

The  $\Phi_+$  is a function of  $x - ct$ , therefore it must be constant along any line  $x - ct = \text{constant}$ . Such line is called characteristic and speed  $c$  is the slope of the characteristic (Abbot and Minns, 1998, Durran, 1999). In the finite difference domain a characteristic located between two spatial grid points at the old time step can be followed to predict the value of  $\Phi_+$  at the new time step. Similar conclusion can be deduced with respect to  $\Phi_-$ .

The variables  $\Phi_+$  and  $\Phi_-$  can be also used to construct two equations instead of eqs. (1) and (2),

$$\frac{\partial \Phi_+}{\partial t} + c \frac{\partial \Phi_+}{\partial x} = 0 \quad (27)$$

$$\frac{\partial \Phi_-}{\partial t} - c \frac{\partial \Phi_-}{\partial x} = 0 \quad (28)$$

These will better serve for the boundary condition construction since the values of  $\Phi_+$  and  $\Phi_-$  are preserved along characteristics.

Consider, the wave propagation in a channel with the left end located at  $x = 0$  and the right end at the distance  $x = L$ . From the left end enters a wave denoted as  $\Phi_+$ , it propagates towards the right end. If the right boundary ought to be transparent to this wave the requirement is that there will be no reflection, or  $\Phi_- = 0$ . From eq.(26b) it follows that the sea level at the right end of the channel is

$$\zeta = u\sqrt{H/g} \quad (29)$$

Similarly, if the left end of channel ought to be transparent for an incoming wave, eq. (26a) will prescribe the sea level under condition that  $\Phi_+ = 0$

$$\zeta = -u\sqrt{H/g} \quad (30)$$

Problem to solve is a construction of semi-transparent boundaries, when e.g., at the left-hand boundary a permanent signal is generated and the right-hand boundary is the reflective one. A signal, reflected from the right boundary when arriving to the left boundary must find the way out because if this boundary is not transparent the reflected signal will pump energy causing permanent increase of the amplitude in the channel. To this purpose, can serve eq. (26a), assuming that incoming wave from the left boundary is constant  $\Phi_+ = Const$ , the relations between amplitude and velocity follows. There are a few variations of this approach e.g., setting sea level at the left boundary as a constant and calculating  $\Phi_+$  and  $\Phi_-$  along characteristics in proximity to the boundary and afterwards inserting this values for the boundary conditions to calculate velocity from eq.(23).

In many applications, while going from the larger-scale domain to the smaller-scale, the open boundary for the smaller domain are taken from the larger scale computations or observations. Suppose at the left-hand boundary the sea level ( $\zeta_b$ ) and velocity ( $u_b$ ) are given either from measurements or computations. The incoming value of the  $\Phi_+$  is defined as

$$\Phi_+ = \frac{\zeta_b + u_b\sqrt{H/g}}{2} \quad (31)$$

and for the smooth propagation into domain this value ought to be equal to the invariant specified inside computational domain in the close proximity to the boundary

$$\Phi_+ = \frac{\zeta + u\sqrt{H/g}}{2} \quad (32)$$



or,

$$\zeta = \zeta_b + (u_b - u)\sqrt{H/g} \quad (33)$$

Some understanding of the above condition can be gleaned by comparison to the radiation conditions given by eqs. (29) and (30). Generally eq.(33) requires that at the boundary, calculated variables in the smaller domain be equal to the measured (or input variables). One cannot expect this condition to be fulfilled at the initial stage of a computation, especially when the computation start from zero velocity. The second term at the right-hand-side of eq.(33) is actually a radiation condition, which radiates difference between prescribed and computed velocity. When stationary conditions will be achieved the difference of velocity will be close to zero. Condition (33) is often used to establish open boundary condition for the tidal computations (Flather, 1976). The usefulness of eq.(33) for the transient tsunami processes requires further testing.

## 6. Numerical implementation of the boundary condition

Fig. 10 depicts grid distribution at the left-hand boundary. Two-time level numerical scheme is considered. Both sea level and velocity are having the same space index. Let's start by considering radiation boundary condition defined for the velocity. Here a simple implementation of eq.(30) reads,

$$u^{m+1} = -\zeta_1^{m+1}\sqrt{g/H} \quad (34)$$

The question to be answered is that eq.(34) is actually valid along the characteristic and not at the grid points. First, it is useful to notice that this radiating condition is also fulfilled by the equation for the sea level

$$\frac{\partial \zeta}{\partial t} - c \frac{\partial \zeta}{\partial x} = 0 \quad (35)$$

and thus the value of the sea level is constant along the characteristic which propagates from the old time ( $m$ ) into the new time ( $m + 1$ ) domains as shown in Fig. 10 by dashed line. The distance  $dx = cT$ , where  $c$  denote phase velocity and  $T$  is time step. The sea level at the old time step is defined at the point  $p$  on the characteristic,

$$\zeta_p = \frac{\zeta_1^m(h - dx) + \zeta_2^m dx}{h} \quad (36)$$

This sea level is equal to the sea level at the new time step ( $\zeta_1^{m+1} = \zeta_p$ ), and since  $dx = cT$ , and time step and space step are given; denoting  $cT/h$  as  $\gamma$ , the above equation can be written as,

$$\zeta_1^{m+1} = \zeta_1^m(1 - \gamma) + \zeta_2^m \gamma \quad (37)$$

Eq.(37) can be introduced into (34) to calculate velocity. Notice that this velocity is defined in the sea level point ( $j = 1$ ). Calculations show that actually (34) works quite well even if the variables are defined in the grid points and not along the characteristics.

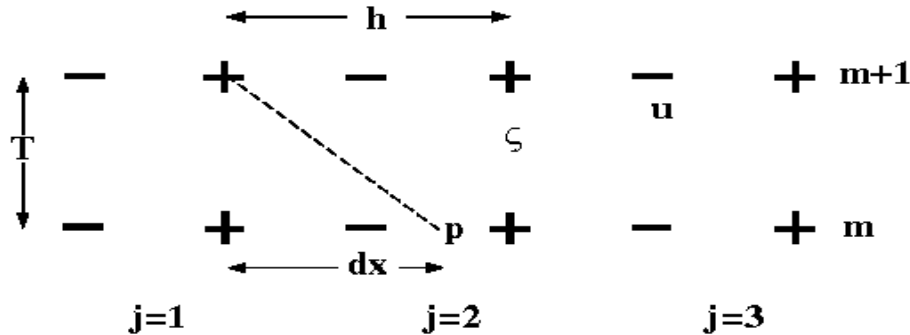


Figure 10

The boundary conditions defined through the modeling or observations require also smooth transition between conditions and computed variables. To this purpose serves well eq.(33); at the left boundary it can be written as (assuming sea level is prescribed at the  $j=1$  grid point and velocity at the  $j=2$  grid point),

$$\zeta_1^{m+1} = \zeta_b^{m+1} + (u_b^{m+1} - u_2^{m+1})\sqrt{H/g} \quad (38)$$

The major problem arises when only one variable is given at the open boundary: sea level or velocity. With such condition an incoming characteristic is not fully defined, therefore the above relation cannot be applied. It is easy to start computation with the prescribed sea level but when the reflected wave arrives to the open boundary and its magnitude differs from the open boundary value, the energy build up ensue resulting in an instability. Several solutions are feasible but none is resolving the problem completely. Generally, a difference between the prescribed sea level magnitude at the boundary and the sea level generated by the reflected wave at the same boundary is due to an initial adjustment problem or due to transient character of the signal. The prescribed boundary condition should actually include both incoming and outgoing signal. One possible solution for arriving at the stationary signal, is to introduce the radiating mechanism into a boundary condition and slowly remove this mechanism in time. Assume, at the left boundary the amplitude is prescribed as  $\zeta_1^{m+1} = a \cos \omega(m+1)T$ , now introducing accordingly to eq.(30) a radiating signal, the boundary condition at the left boundary reads,

$$\zeta_1^{m+1} = a \cos \omega(m+1)T - u_2^{m+1}\sqrt{H/g} \quad (39)$$

The second term at the right-hand-side of the above equation ought to be slowly removed in time after the initial adjustment process is over. If only the sea level ( $\zeta_b^{m+1}$ ) is given

at the boundary a different approach can be worked out starting from eq.(38). The new boundary value ( $\zeta_1^{m+1}$ ) at the same grid point can be calculated by the radiation condition, using, e.g., eq.(37). This sea level will differ from prescribed boundary value  $\zeta_b^{m+1}$ . The difference may be used to calculate a correction for the boundary value of velocity at the point  $j = 2$ . We rewrite eq.(38) as

$$u_{2,c}^{m+1} = u_2^{m+1} + \sqrt{g/H}(\zeta_b^{m+1} - \zeta_1^{m+1}) \quad (40)$$

Velocity  $u_2^{m+1}$  has been computed in the regular way, i.e., by application of  $\zeta_b^{m+1}$  as the boundary value.

### Acknowledgments

This study was supported by the Arctic Region Supercomputing Center at the University of Alaska Fairbanks. I am indebted to my students Juan Horrillo and Elena Suleimani for their help and discussions throughout the work.

### References

- Abbot, M.B. and A.W. Minns. 1998. *Computational Hydraulics*. Ashgate, Aldershot, 557pp.
- Durrant, D.R. 1999. *Numerical Methods for Wave Equations in Geophysical Fluid Dynamics*. Springer, 465pp.
- Flather, R.A. 1976. A tidal model of the north-west European continental shelf. *Mem. Soc. R. Sci. Liege*, **6**, 141–164.
- Flather, R.A. and Heaps, N.S. 1975. Tidal computations for Morecambe Bay. *Geophys. J. Royal Astr. Soc.*, **42**, 489–517.
- Imamura F. 1996. Review of tsunami simulation with a finite difference method. In *Long-Wave Runup Models*, H.Yeah, P. Liu and C. Synolakis, Eds, World Scientific, 25–42.
- Kowalik, Z. 2001. Basic relations between tsunami calculation and their physics, *Science of Tsunami Hazards*, **19**, 2, 99–115.
- Kowalik, Z. and I. Bang. 1987. Numerical computation of tsunami run-up by the upstream derivative method. *Science of Tsunami Hazards*, **5**, 2, 77–84.
- Kowalik, Z. and Murty, T.S. 1993a. *Numerical Modeling of Ocean Dynamics*, World Scientific, 481 pp.
- Kowalik, Z. and Murty, T.S. 1993b. Numerical simulation of two-dimensional tsunami runup. *Marine Geodesy*, **16**, 87–100.
- Lewis, C.H. III and Adams, W.M. 1983. Development of a tsunami-flooding model having versatile formulation of moving boundary conditions. *The Tsunami Society MONOGRAPH SERIES*, No.1, 128 pp.
- Lynett, P.J., Tso-Ren Wu and P. L.-F. Liu. 2001. Modeling wave runup with

depth-integrated equations. Submitted to Coastal Engineering.

Mader, C. L. 1986. *Numerical Modeling of Water Waves*, Univ. Calif. Press, Berkeley, Los Angeles, 206 pp.

Parker, B. B. 1991. The relative importance of the various nonlinear mechanisms in a wide range of tidal interactions (Review). In: *Tidal Hydrodynamics*, B. B. Parker, Ed., Wiley and Sons, 237–268.

Reid, R.O. and B.R. Bodine. 1968. Numerical model for storm surges in Galveston Bay. *J. Waterway Harbour Div.*, **94**(WWI), 33–57.

Titov, V.V. and Synolakis, C.S. 1998. Numerical modeling of tidal wave runup. *J. Waterway, Port, Coastal and Ocean Eng.*, **124**, 4, 157–171.